ACS NANO

www.acsnano.org

ARTICLE

High-Speed Spectral Characterization of Single-Molecule SERS Fluctuations

Makayla M. Schmidt,[▽] Emily A. Farley,[▽] Marit A. Engevik,[▽] Trey N. Adelsman, Ariadne Tuckmantel Bido, Nathan D. Lemke, Alexandre G. Brolo,* and Nathan C. Lindquist*

Cite This: *ACS Nano* 2023, 17, 6675−6686

Read Online

ACCESS | Metrics & More | Article Recommendations | Supporting Information

ABSTRACT: The concept of plasmonic "hotspots" is central to the broad field of nanophotonics. In surface-enhanced Raman scattering (SERS), hotspots can increase Raman scattering efficiency by orders of magnitude. Hotspot dimensions may range from a few nanometers down to the atomic scale and are able to generate SERS signals from single molecules. However, these single-molecule SERS signals often show significant fluctuations, and the concept of intense, localized, yet static hotspots has come into question. Recent experiments have shown these SERS intensity fluctuations (SIFs) to occur over an extremely wide range of timescales, from seconds to microseconds, due to the various physical mechanisms causing SERS and the dynamic nature of light−matter interaction at the nanoscale. The underlying source of single-molecule SERS fluctuations is therefore likely to be a complex interplay of several different effects at different timescales. A high-speed acquisition system that captures a full SERS spectrum with microsecond time resolution can therefore provide information about these dynamic processes. Here, we show an acquisition system that collects at a rate of 100,000 SERS spectra per second, allowing high-speed characterization. We find that while each individual SIF event will enhance a different portion of the SERS spectrum, including a single peak, over 10s to 100s of microseconds, the SIF events overall do not favor one region of the spectrum over another. These high-speed SIF events can therefore occur with relatively equal probability over a broad spectral range, covering both the anti-Stokes and the Stokes sides of the spectrum, sometimes leading to anomalously large anti-Stokes peaks. This indicates that both temporally and spectrally transient hotspots drive the SERS fluctuations at high speeds.

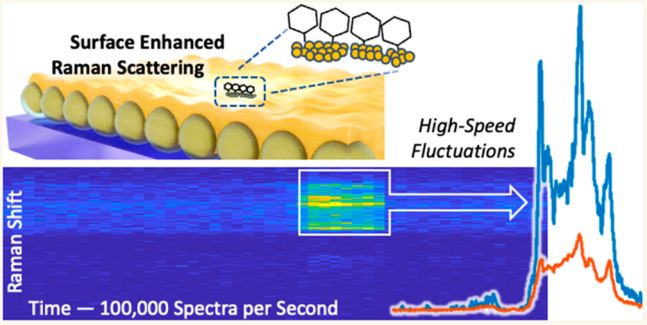

KEYWORDS: *Surface Enhanced Raman Spectroscopy (SERS), Single Molecule SERS, High-Speed Fluctuations, Plasmonic Hotspots, High-Speed Spectroscopy*

Illuminating metallic nanostructures creates areas of intense electromagnetic fields called hotspots.[1] These intense and highly localized fields are generated by the excitation of localized surface plasmon resonances (LSPRs). This effect enhances light−matter interaction and gives rise to a broad range of surface-enhanced effects with important applications, such as developing fast and efficient biosensors,[2] triggering chemical reactions on the nanoscale,[3] creating optoelectronic devices,[4] or exploring two-dimensional materials.[5] The surface-enhanced Raman spectroscopy (SERS) effect in particular is a phenomenon that effectively represents both the challenges and opportunities inherent to nanophotonics and the study of light−matter interactions at the nanoscale.[6] Experiments over several decades have shown that SERS signals are many orders of magnitude stronger than from normal Raman scattering alone for a given number of molecules and illuminating laser power.[7,8] These enhanced signals can even originate from single molecules.[9,10] Central to the interpretation of the SERS effect is the concept of a plasmonic hotspot[11] with nanometric, and perhaps even atomic, dimensions.[12,13] LSPR of metallic nanoparticles and nanostructures is well-studied and understood, and much effort has gone into designing SERS substrates with high enhancement factors.[14] However, hotspots able to generate a single molecule response are thought to be created by the excitation of hyper-localized hotspots whose resonance behavior depends on the geometric features at the local

Received: December 15, 2022
Accepted: March 17, 2023
Published: March 23, 2023

https://doi.org/10.1021/acsnano.2c12457
ACS Nano 2023, 17, 6675−6686

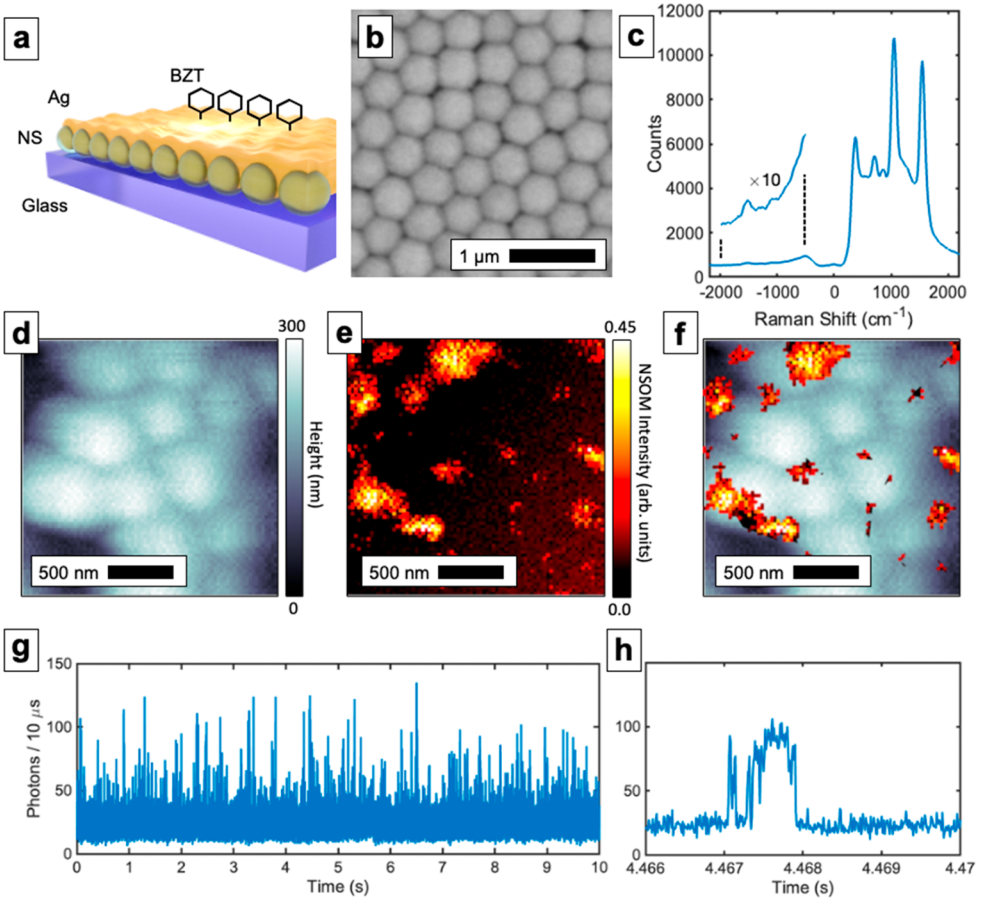

Figure 1. High-speed signal fluctuations from SERS substrate. (a) Illustration of benzenethiol (BZT) molecules coating an Ag film-over nanosphere (FoN) sample. (b) SEM image shows the roughness and gaps of the substrate for good SERS activity. (c) Representative SERS spectrum of the substrate, showing both the Stokes and the anti-Stokes regions. The peaks on the anti-Stokes side are smaller. (d) Height scan of the sample with (e) a corresponding NSOM image of the SERS light, showing a distribution of hotspots over the surface. (f) Composite height map and NSOM image of the sample. (g) Representative SERS intensity−time trajectory recorded with a separate photon counting module and (h) zoomed in region showing high-speed SERS fluctuations. In this case, only the overall intensity of the SERS signal is recorded and spectral information is lost.

nanoenvironment, including the local arrangement of metallic adatoms or nanometric protrusions and any proximate molecules, as well as the broader LSPR of the larger nanoparticle or nanodevice.[15] Indeed, while much progress has been made,[16] the complex nature of the different contributions to the SERS effect requires well-defined experimental protocols at multiple timescales to explore the intrinsic nonuniformities of the hotspot distributions on SERS substrates. For example, one of the hallmarks of single-molecule SERS is a pervasive fluctuation or blinking effect[9] in the overall signal intensity.[17,18] Recent experiments performed with high-speed imaging revealed that these SERS intensity fluctuations (SIFs) occur over a wide range of timescales, from tens of seconds down to single microseconds.[19] Super-resolution imaging and experiments with multiple laser wavelengths and polarization states[20] showed that SIFs occur on the subnanoparticle level in hyper-localized (<10 nm) regions of larger nanoparticles or aggregates (~100 nm). These intensity fluctuations occur in different combinations of probe molecule and nanoparticle shape, size, and material and appear to be a fundamental characteristic of the SERS effect.[21] Furthermore, local environmental differences such as probing molecules dried onto the surface or those freely diffusing in liquid also reveal the complexity of the metal/molecule/hotspot system with Brownian motion and trapping forces playing a role in the high-speed dynamics.[22]

However, not only the intensity but also the spectral features of the SERS signals are known to fluctuate in time,[23] and high-speed SERS spectroscopy (in the μs range) has not yet been fully explored. The spectral content of SERS obtained at high speeds would provide a fuller picture of fluctuation behavior compared to examining just the intensity. In this paper, we show an acquisition system that collects at a rate of more than 100,000 SERS spectra per second, allowing high-speed spectral characterization to provide clues to the underlying physical mechanisms. Since most SERS experiments are done within the ~10 ms to 1 s timescales, given by the integration times and frame rates of a typical CCD camera, our system offers faster acquisition rates of full SERS spectra. These high-speed acquisitions reveal intense spectral features that fluctuate on the 10s of microseconds timescales. While each individual SIF event will enhance a portion of the SERS spectrum, including a single peak, over 10s to 100s of microseconds, we find that the SIF events overall do not favor one region of the spectrum over another. These high-speed SIF events can therefore occur with relatively equal probability over a broad spectral range, covering both the anti-Stokes and the Stokes sides of the spectrum. This

https://doi.org/10.1021/acsnano.2c12457
ACS Nano 2023, 17, 6675−6686

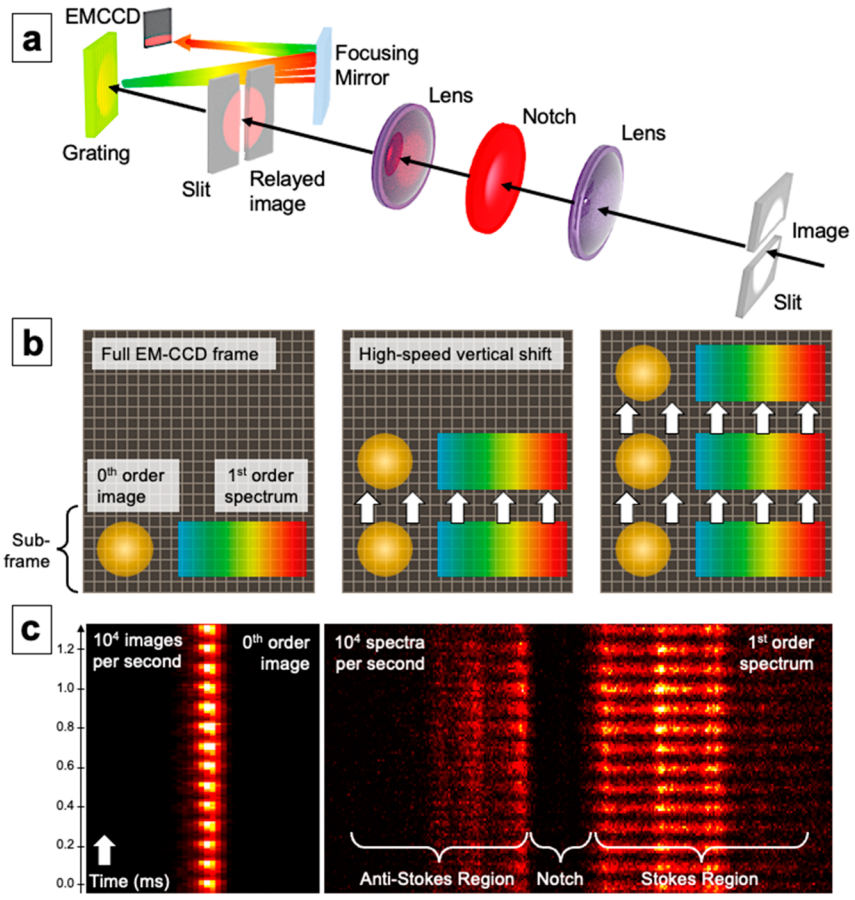

Figure 2. High-speed spectral acquisition system. (a) Optical setup with SERS light traveling from a microscope image through slits, lenses, a notch filter, and a grating to a high-speed camera. (b) The camera performs a sequence of high-speed vertical shifts of a subframe along the *y*-axis, and spectral data is dispersed along the *x*-axis. (c) Raw data from the high-speed acquisition system. The zeroth order from the grating shows a filmstrip of the particle image while the first order shows the SERS spectrum.

indicates both temporally and spectrally transient hotspots driving the SERS fluctuations at high speeds.

RESULTS AND DISCUSSION

SIF behavior has been shown to occur in a wide variety of SERS experiments and sample types.[24] Here, we use a well-known and relatively simple substrate shown in Figure 1a. The sample consisted of a 300 nm thick silver film over nanosphere (FoN) substrate with 500 nm diameter silica nanospheres. Figure 1b shows a scanning electron microscope (SEM) image of a characteristic FoN sample, and Figure 1c shows a representative SERS spectrum from the sample, with both the Stokes and anti-Stokes regions. The intensities in the Stokes region are much higher than the anti-Stokes region and shows strong peaks near ∼1000 and ∼1570 cm^{-1}, consistent with the spectrum of BZT.[25] The 660 nm excitation laser was filtered with a high-efficiency notch filter, and all spectra were recorded on an electron-multiplied (EM) CCD camera attached to an imaging spectrometer. The EMCCD camera was deep-cooled to operate in a single-photon counting mode with low noise. Although the resolution of the spectrometer is relatively low with a 100 line/mm grating, it can gather a wide range of the full SERS spectrum from around −2200 to +2200 cm^{-1} while maintaining the relevant spectral features and providing a good signal-to-noise ratio. Several laser powers were used for the various experiments. For a 1 s "long exposure" SERS spectrum shown in Figure 1c, a power of ∼0.1 mW at the sample was used with a 100× (NA = 0.9) objective. This created a focal spot of roughly ∼400 nm in diameter and a power density of ∼10^9 W/m^2. Experiments with the shortest exposure times and highest EMCCD gains used laser powers of around ∼1 mW at the sample. While many single-molecule SERS experiments are done with low laser powers, sample damage was minimized by using thick silver films. The metal film in our samples acted as a heat sink,[26] allowing higher laser powers to be used for a short time during the higher acquisition speed experiments.

Generally, a SERS substrate will have roughness features that provide a good distribution of hotspots. A typical hotspot distribution in our samples was characterized using a near-field scanning optical microscope (NSOM). Briefly, a 638 nm laser was fiber-coupled into a 200 nm diameter NSOM probe to collect SERS signals from the sample with a photon counting module and a long-pass filter. Figure 1d shows the height scan of the sample with the corresponding NSOM map shown in Figure 1e. A composite image in Figure 1f shows that the hotspots are arranged randomly over the surface, although the largest most intense hotspots are between the nanospheres or on the edges. This random distribution of hotspots provides significant, though nonuniform, SERS intensity across the sample and forms the basis for our single-molecule SERS experiments.

Figure 1g shows a SERS time trajectory from our inverted microscope when an illuminating 660 nm laser is focused onto a single area with good SERS signal. The signal is collected by a high-speed photon counting module. Over the course of several

https://doi.org/10.1021/acsnano.2c12457
ACS Nano 2023, 17, 6675−6686

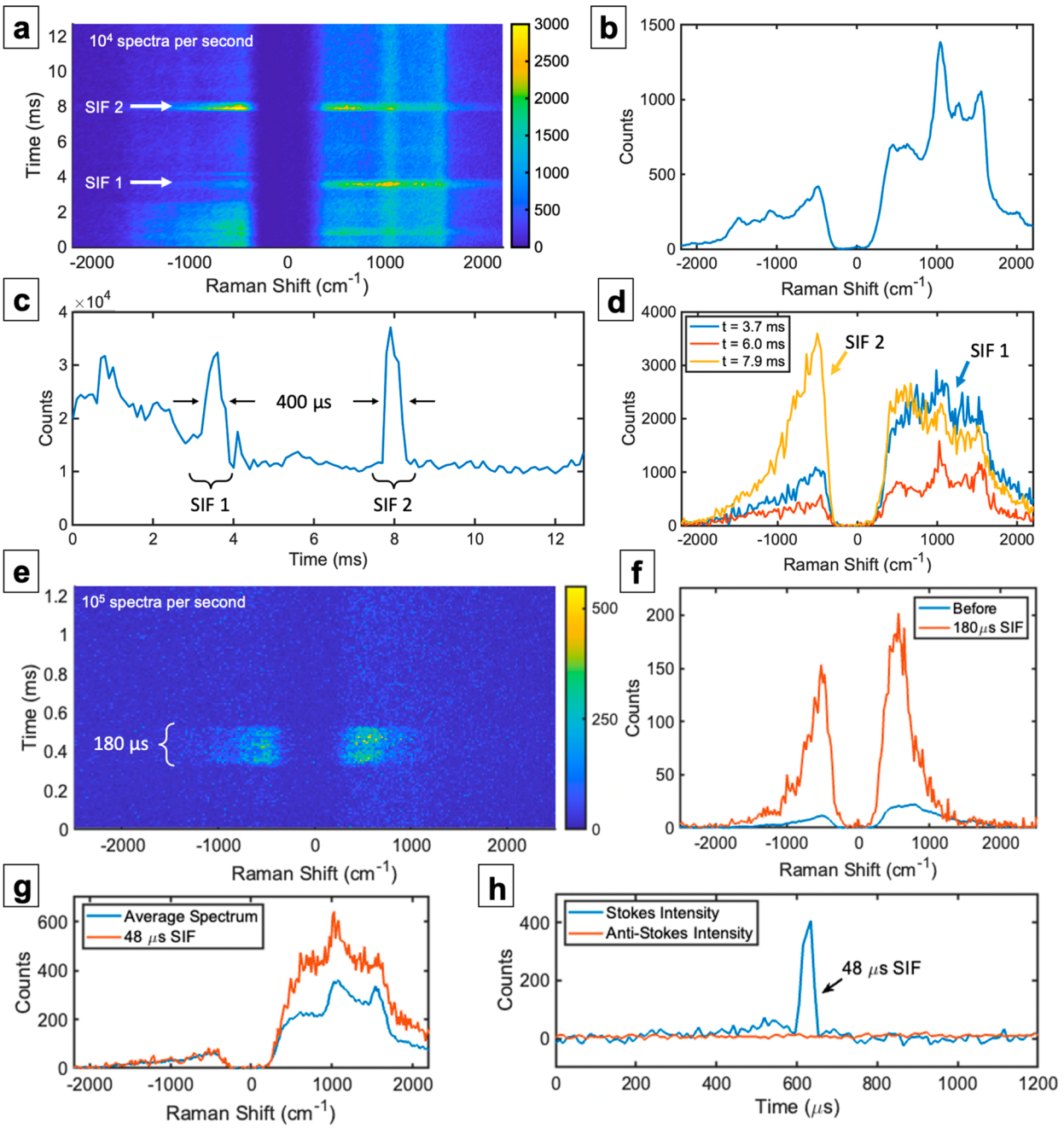

Figure 3. Need for spectral characterization. (a) Waterfall plot of high-speed SIF events recorded at 10^4 spectra per second. (b) Integrating the waterfall plot in time for an equivalent 12.8 ms integration-time spectrum gives a high-quality SERS spectrum but loses all time dynamics that happen on a scale faster than the integration time. (c) Intensity trajectory of the SERS signal, again showing high-speed SIF events. (d) The spectral information from each SIF and a time step in between reveals that each SIF event has a different spectral shape that is not available in the intensity trajectories. (e) Faster scanning at 10^5 spectra per second captures a brief 180 μs event. (f) The spectrum of this flare-type event is broad and relatively featureless and extends across both the Stokes and anti-Stokes regions, with the notch blocking the central portion. (g) Another SIF event taken at 10^5 spectra per second. In this case, only the Stokes side of the SERS spectrum is enhanced during the SIF, shown clearly in (h) a time trajectory of the average intensity in each spectral region.

seconds, the SERS signal is seen to experience significant and rapid fluctuations. Figure 1h shows that these fluctuations can occur on submillisecond timescales. Generally, the signal fluctuations are thought to arise from the probe molecules moving into and out of a static hotspot, the hotspot itself forming and unforming due to motion of the metallic adatoms on the nanostructures or a combination of both of these effects.[24] While a point-like, single-pixel photon counting module can characterize the timing of these fluctuations and an array of point detectors could provide an image,[19] high-speed spectral information has not yet been fully explored.

High-speed spectral acquisition is accomplished by using the EMCCD camera programmed in a mode that records only a small strip of pixels at a time. Figure 2a shows the optical setup with slits, a notch filter, the spectrometer grating, and the EMCCD array. For maximum sensitivity, the EMCCD array was run in a single photon-counting mode and deep-cooled to −70 °C. Since light is only illuminating a bottom strip of the pixel

https://doi.org/10.1021/acsnano.2c12457
ACS Nano 2023, 17, 6675−6686

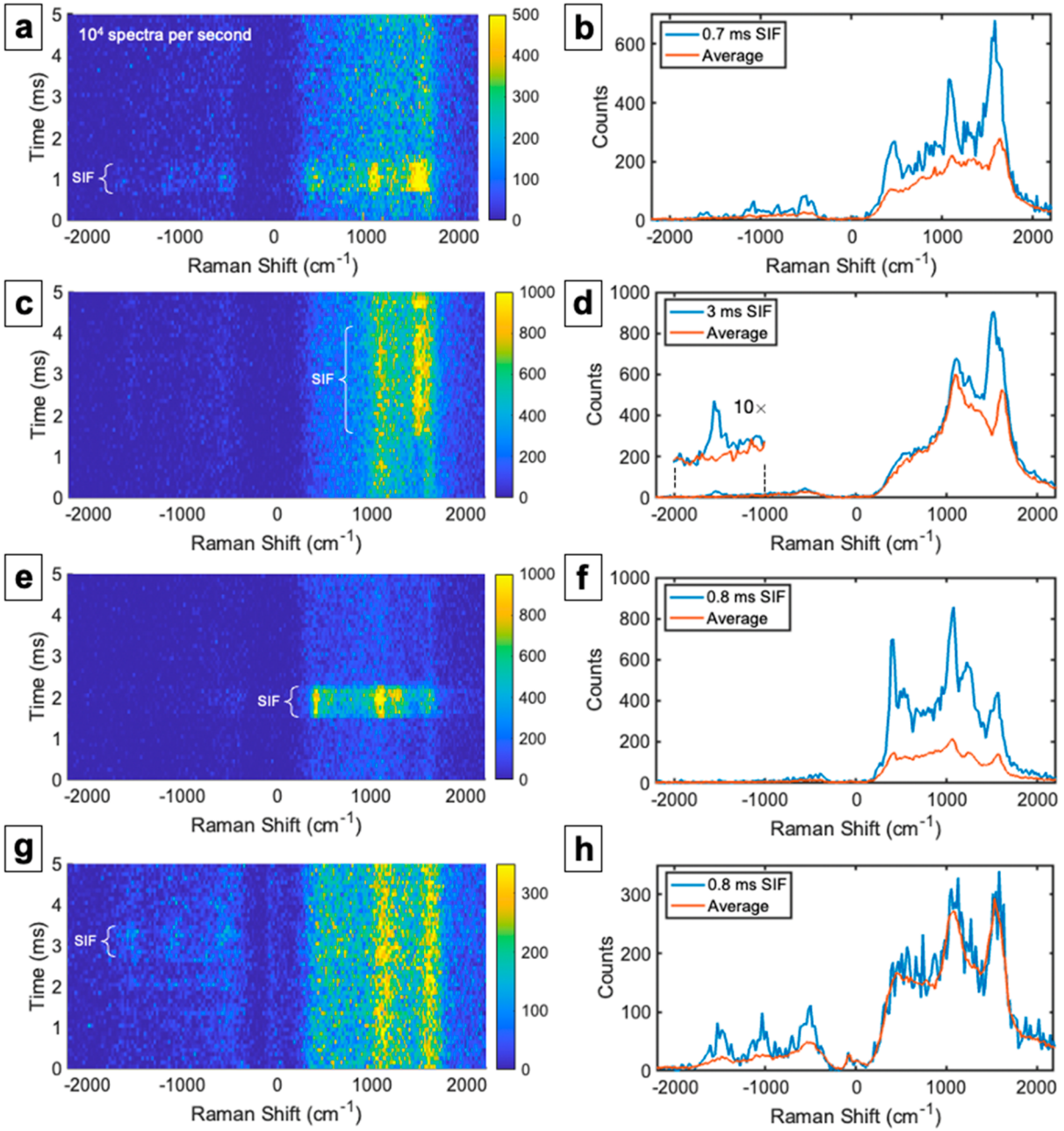

Figure 4. Various SIF events with spectral content recording at 10^4 spectra per second. (a) Waterfall plot of a SIF event that involves both (b) the Stokes and anti-Stokes regions. (c) Waterfall plot of a SIF event that involves primarily (d) a single peak in the Stokes and anti-Stokes regions near ± 1570 cm^{-1} while the rest of the spectrum remains fairly stable. (e) Waterfall plot of a SIF event that involves mostly (f) the entire Stokes region. (g) Waterfall plot of a SIF event that involves mostly (h) the entire anti-Stokes region.

array, due to closing the slits, data can be stored in the rest of the imaging pixels themselves without being corrupted. To start the process, the camera collects light on the pixel strip for a set integration time. Immediately after, this pixel strip is shifted vertically into the next segment and stored, shown in Figure 2b. After a number of vertical shifts, the entire pixel array is finally read out in a normal fashion, giving a "filmstrip" series of images of the sample in time. In this way, the acquisition speed is limited by the rate of internal vertical shift speed of the EMCCD, which in our camera was 0.6 μs, added to the exposure time of the pixels needed for sufficient signal. With this scheme, the vertical field-of-view is limited, but the entire width of the EMCCD array can be used for imaging and spectroscopy. A typical setting for our camera digitized an 8 × 1024 pixel strip. This allowed 128 strips to be stored in the entire 1024 × 1024 pixel array, representing a short burst of spectral data vs time that exceeds the typical throughput of the camera running in a full-frame mode. Vertical shift rates and exposure times were used to give acquisition rates of 10,000 spectra per second or 100,000 spectra per second, depending on the experiment. Figure 2c shows raw data from a typical scan. Since the light passes through an imaging spectrometer, the zeroth order from the grating provides an image of the particle shown on the left "filmstrip" region, and the first order disperses the SERS spectrum, both the Stokes and anti-Stokes regions, shown on the right "filmstrip" region. The zero-order image could potentially be used in future experiments to correlate high-speed imaging with high-speed spectroscopy. In the case of Figure 2c, the system is acquiring

https://doi.org/10.1021/acsnano.2c12457
ACS Nano 2023, 17, 6675−6686

10,000 subframe images per second, although this recording mode is again limited by the vertical shift speed of the camera, the chosen pixel exposure time, and the physical size of the pixel array. Finally, sequences of these short bursts were recorded with typical full-frame camera rates of around 30 frames per second. In other words, we collect short bursts of 128 high-speed spectra. These short bursts represent 1.28 or 12.8 ms total scanning time, depending on the overall scan rate.

Figure 3 shows how this high-speed spectroscopy system can be used for studying high-speed SERS fluctuations. Figure 3a shows a waterfall plot of the SERS spectrum, recorded at 10,000 spectra per second for a total time of 12.8 ms. Recording at this high speed will reveal features that are not apparent in the slower, longer integration time shown earlier in Figure 1c. For example, the anti-Stokes side of the spectrum is more enhanced in the $t = 0$ to $t = 3$ ms range and then is reduced. Several other features in the spectrum vs time are seen, labeled as "SIF 1" and "SIF 2" that occur at 3.7 and 7.9 ms, respectively, after the acquisition starts. A constant background spectrum is also seen in the intermediate portions. Averaging the entire spectrum will simulate a longer exposure time of the full 12.8 ms time window. This, of course, averages out the spectral fluctuations that occurred on the faster timescale of Figure 3a but produces a SERS spectrum shown in Figure 3b. Plotting the average intensity vs time of the spectrum produces a SERS time trajectory, shown in Figure 3c, that simulates the high-speed acquisition of a point-like detector but is missing the spectral data. The two SIF events are shown, each lasting around 400 μs. Figure 3d shows the utility of high-speed spectral acquisition, in that the full spectrum can be extracted from each event. While the SIF events look very similar in the time trajectory shown in Figure 3c, the spectral features and shapes are different. Indeed, these events appear to be more of a broadband luminescence or "flare" type event that arises from the metal surface itself and not the molecules.[27] These events are quite common in high-speed SERS experiments, a sample of which is shown in Figure 3e,f, capturing an intense and short-lived 180 μs event. Light emission from metallic nanostructures and nanojunctions is an active area of research whose exact mechanism is still under investigation.[28−31] While "photoluminescence" effects are related to the localized plasmonic resonances that also drive the SERS effect and they contribute to the background in SERS spectra,[30] there are important distinctions that have been explored. For example, super-resolution imaging of nanoparticle aggregates noted a difference in the ways that the extremely localized SERS emission and the wider photoluminescence emission coupled to the higher-order plasmon resonances of the aggregates.[32] Because of this coupling, the photoluminescent background has recently been used as a method of spectral calibration to recover the "true" SERS spectrum.[33] The relationship between fluctuating background photoluminescence and fluctuating SERS emission is also still under investigation. For example, fluctuations of luminescence from gold nanostructures were seen to not correlate to SERS emission, nor to any fluctuations in the dark-field scattering spectra, suggesting different physical origins.[34] In other work, strong fluctuations of photoluminescent "flare" events were seen to be influenced by the formation of atomic-scale hotspots, consistent with descriptions of the fluctuating SERS effect.[27] These types of differences further emphasize the need for spectral analysis of specific peaks to separate luminescence events from high-speed, single-molecule SERS fluctuation events. To elucidate the role of the silver surface, metal luminescence, and "flare"-type events in our experiments, we fabricated an additional Ag-FoN sample but without the BZT incubation step. We found that the bare Ag-FoN surface also exhibited light emission with some fluctuation activity. Some characteristic fluctuation events, as shown already in Figure 3 but now in the absence of the BZT molecules, are shown in Figure S1. While the use of our 660 nm laser will not effectively drive interband electronic transitions in silver and while the physical origin of background light emission, its fluctuation dynamics, and its relationship to the SERS effect is still under investigation, the focus of our current manuscript is to present an analysis of SERS fluctuations using high-speed spectroscopy and analysis of specific peaks. It is distinguishing between such events and features of the spectrum that will give a deeper fundamental insight into the SERS effect and light−matter interaction in the complex metal/molecule/hotspot system. For example, fluctuations in the Stokes side of the SERS spectrum are not always correlated in overall strength to fluctuations in the anti-Stokes side of the spectrum.[35,36] This is shown in Figure 3g, wherein only the Stokes side fluctuates during a 48 μs long SIF event. Plotting the average intensity of both the Stokes and anti-Stokes regions in Figure 3h shows this disparity. Capturing the full spectrum of a SERS fluctuation is therefore critical to more fully understanding the different dynamical processes that contribute to the SERS effect.

A collection of various SIF events is shown in Figure 4. These events involve various portions of the SERS spectrum and can be broadly classified as: (1) involving a broad region covering both the Stokes and anti-Stokes sides, shown in Figure 4a,b; (2) involving a single peak in both the Stokes and anti-Stokes regions, shown in Figure 4c,d; (3) involving the Stokes region only, shown in Figure 4e,f; (4) involving the anti-Stokes region only, shown in Figure 4g,h. These representative SIFs were recorded at 10,000 spectra per second and occur on ∼1 ms timescales. Events shown in Figure 3 were on the 10s of μs timescale, showing the wide range of SIF timing. While our system is limited in the maximum length of SIF that it can record for a given acquisition speed, due to the high-speed burst mode of the camera, previous experiments have shown single SIF events to last from the 10s of microseconds range into the 100s of milliseconds range.[22]

Given the wide variety of spectral features, both in the SERS spectrum and in the broadband background, there appear to be many mechanisms that will cause SIFs to occur. The simplest model is that a hotspot is generated by illuminating the nanometallic surface and subsequently a molecule enters that hotspot,[9] similar to single molecule fluorescence experiments.[10] While "chemical mechanisms" and resonance Raman effects[15] also play a role in enhancing the Raman response from adsorbed molecules,[16,17] this "single molecule entering a single hotspot" interpretation involves a purely electromagnetic enhancement mechanism.[6] Single molecule SERS of this type has been verified through experiments using isotopologues.[27] This would cause an event like that of Figure 4a,b where the entire SERS spectrum suddenly increases. However, in this work, the sample surface is dried and completely saturated with molecules. How a single molecule enters and leaves a single hotspot is not clear. Previous experiments involving dry samples[11] and single nanostructures[12] with surface concentrations much higher than would permit only a single molecule to be illuminated at a time[13] have also observed strong fluctuations. Since it is known that only a small fraction of the adsorbed molecules (∼1%) in a fully coated surface will contribute to the majority of the SERS response over

https://doi.org/10.1021/acsnano.2c12457
ACS Nano 2023, 17, 6675−6686

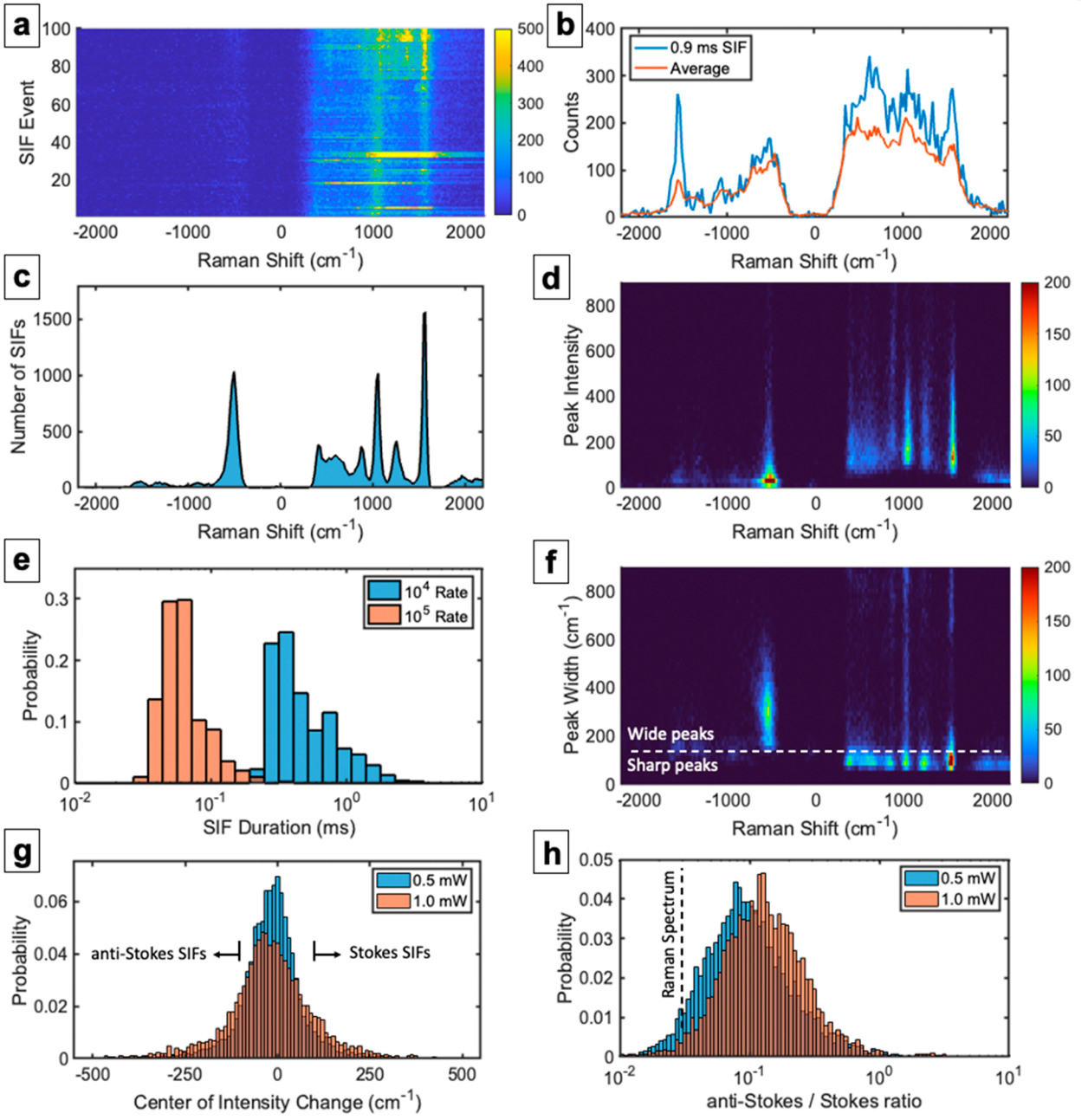

Figure 5. Statistical analysis of SIF events. (a) A stacked series of 100 different SIF events. Each event has a distribution of peaks and spectral features. (b) A sample SIF event with a large increase in a single anti-Stokes peak. (c) Locating the peaks in each SIF using a peak fitting algorithm shows a histogram distribution of peak locations. The peak at 1570 cm^{-1} is the most common peak to detect in the Stokes region across all SIFs. The large peak around −500 cm^{-1} is an artifact due to the shoulder of the notch filter. (d) A two-dimensional histogram showing the intensity distribution of all detected peaks in all SIF events. Most SIF events have a peak height of a few hundred counts, although some SIF events have peak heights nearly 10 times higher. (e) Histogram of the detected SIF event durations for the two recording speeds. While each recording speed has a maximum SIF duration that is detectable due to the limited number of frames, the SIF events cover a wide range of timescales from 10s of μs to 10s of ms. (f) Histogram of the widths of the detected peaks. Most peaks are sharp, i.e., around the resolution of the spectrometer of ∼100 cm^{-1}, although many detected peaks are much wider. (g) Histogram of the relative change in the center of intensity of the entire spectrum. Three distinct regions can be defined corresponding to SIF events that occurred primarily in the Stokes region, primarily in the anti-Stokes region, or in both simultaneously. (h) A log histogram of the average anti-Stokes to Stokes ratio of each SIF event. Higher laser powers generated a higher relative anti-Stokes intensity, although there is a wide distribution. The vertical dashed line is the ratio of the regular Raman spectrum shown in Figure S8.

a large area,[23] it is reasonable that a highly efficient hotspot could generate a single-molecule signal on a dried sample, but perhaps due to the generation of the hotspot at the molecule rather than the molecule entering a hotspot. Recent experiments of high-speed SERS in dry vs aqueous environments have elaborated on this difference.[22]

Figure 4c,d shows a different type of SIF event where it is largely a single peak in both the Stokes and anti-Stokes that is preferentially enhanced. Recent work at cryogenic temperatures

https://doi.org/10.1021/acsnano.2c12457
ACS Nano 2023, 17, 6675−6686

with a scanning probe tip, i.e., tip-enhanced Raman scattering (TERS), has shown submolecular spatial resolution and preferential enhancement of single vibrational modes in a complex molecule by the movement of the tip's hotspot.[37] While further research is needed, these high-speed experiments done at room temperature potentially show that atomic-sized hotspots are intense enough to allow a similar effect. Since the BZT molecules are dried on the silver surface and significant lateral motion of the molecules is unlikely, it is conceivable that rotational reconfiguration of the molecules in place could also induce some of the fluctuation dynamics we observe, including changes in the scattering cross sections from specific vibrational modes.

Figure 4e,f shows yet another type of high-speed SIF wherein the entire Stokes side is enhanced much more than the anti-Stokes side. This is thought to be due to the local resonance of the hotspot. The classical understanding of the SERS effect relies on resonant enhancement due to a broad surface plasmon resonance (SPR) or localized surface plasmon resonance (LSPR) of the nanostructure of both the incoming laser light and the outgoing Raman shifted light. In other words, the resonance width needs to cover both the laser and the entire Raman spectral range. Since typical plasmon resonances can be >100 nm wide in the visible range, Raman shifts over ±3000 cm^{-1} can be resonantly enhanced. Our samples show a broad reflection dip as shown in Figure S2. However, if a localized hotspot resonance only favors a portion of the Stokes or anti-Stokes region, that area will be preferentially enhanced over the rest of the spectrum.[35] This effect is shown again in Figure 4g,h where the anti-Stokes side of the spectrum is enhanced rather than the Stokes side and lasts less than 1 ms. Differential enhancements for Stokes and anti-Stokes scattering during SIFs have been reported by several groups but at slower timescales.[13] The imbalance in the anti-Stokes to Stokes ratios, relative to what is expected from a thermal Boltzmann distribution as discussed further below, has been attributed to several origins, including local heating, local resonances,[38] and optical pumping.[39−41] The timescale of the high-speed fluctuations, in this case only 800 μs long, seems to exclude the possibility of direct thermal effects, since those should occur at longer times as the nanoparticle and substrate heat up or cool down. The results can then be assigned to hotspot resonances that are created and destroyed due to reconstruction of the nanoparticle surface. Similar results were observed for a "nanoparticle in a mirror" system, although at slower timescales.[13] It was suggested that the fluctuations in that case were due to surface reconstructions that led to the formation of pico-cavities within the plasmonic resonance of the larger nanoparticle. Given these considerations, many of the high-speed SIF events shown in Figure 4 may therefore be "hotspot-driven" rather than "molecule-driven" in that the time dynamics and spectral resonances of the hotspot itself broadly influence the spectral features.

Using the high-speed spectroscopy technique, we examined an AgFON sample using a laser power of ∼0.5 mW, recorded at 10,000 spectra per second, and detected each SIF from the raw camera data using a "cumulative sum" anomaly detection algorithm that we have described earlier.[19] Multiple parameters from each SIF event were then extracted such as the SIF duration, the location of the peaks within the SIF, and whether the SIF was captured on the Stokes or anti-Stokes side of the laser line. We used the "findpeaks" peak detection algorithm in MATLAB to detect all peaks above a certain threshold in the spectrum and return their height, location, width, and relative prominence, as shown in Figure S3. This analysis resulted in a set of 6,807 SIFs in total, a sampling of which is shown in Figure 5a. Many peaks are visible, with various relative intensities. A particularly interesting SIF is shown in Figure 5b wherein a single peak at −1570 cm^{-1} in the anti-Stokes region is relatively more enhanced over the rest of the spectrum, lasting only 900 μs. These types of events, which are discussed further below, are rare yet still accessible with high-speed spectroscopy. Figure 5c shows the locations of all detected SIF peaks in the data set from Figure 5a. This histogram essentially recovers the SERS spectrum but is a representation of the number of times a certain peak was detected, not the intensity of that peak. This analysis shows that the most common peaks detected are at +1000 and +1570 cm^{-1} in the Stokes region, although many other peaks were also detected. The large peak on the anti-Stokes side around −500 cm^{-1} is an artifact due to the shoulder of the notch filter. A two-dimensional histogram for all detected SIF peaks is shown in Figure 5d. There is a wide range of individual peak intensities, with some SIFs showing peak intensities that are ∼10 times larger than the same peak in a different SIF. This is represented by the vertical smearing of the histogram. This also shows that the anti-Stokes peaks are generally much smaller than the Stokes peaks, although there are many detected anti-Stokes peaks that are quite large, like the SIF event shown earlier in Figure 5b.

We then examined a set of 11 different Ag-FoN samples, scanning each sample over multiple areas with several different laser powers. The SERS samples are inherently random and heterogeneous, with some locations producing little to no fluctuation activity and other locations producing significant SIF activity. Therefore, to capture as many SIF events as possible, measurements on several samples were taken from many different locations. In all, we fabricated and measured 11 different SERS samples and measured hundreds of different locations, totaling more than 1000 different scans. We captured a set of 84,517 SIF events recorded at 10,000 spectra per second and another set of 21,434 SIFs recorded at 100,000 spectra per second. The highest acquisition speeds required sufficient laser power to collect a SERS spectrum. While our thick Ag-FON substrate could act as a heat sink, photodamage or photodecomposition of the BZT molecules was a possibility at these higher laser powers. At laser powers less than ∼1 mW, the SERS spectrum showed minimal evidence of carbon contamination with well-defined BZT peaks as shown in the previous figures. To probe the stability of the samples and the repeatability of SIF occurrence, we ran slower and longer spectral scans with ∼0.1, ∼0.5, and ∼1.0 mW of laser power, shown in Figures S4, S5, and S6, respectively. The scan rate was 100 spectra per second and ran for 150 s total. The laser dwelled in the same location on the sample for each power scan. While we were not able to resolve the fast time dynamics at this longer timescale, these scans still show significant SIF activity, stability over many minutes for the various laser powers, and that the SIF events are reversible with the spectrum reverting to a stable background without significant or permanent changes or damage. At laser powers much higher than ∼1 mW, the SERS spectrum began to show evidence of contamination. This "burning" effect is shown in Figure S7, with particularly prominent peaks appearing at around ±1300 cm^{-1}, consistent with amorphous carbon clusters.[42] Indeed, photodecomposition of probe molecules has been a source of controversy since carbon contamination can also lead to rapidly fluctuating signals and complicate the picture of single-molecule SERS.[43] However, due to the high-

https://doi.org/10.1021/acsnano.2c12457
ACS Nano 2023, 17, 6675−6686

speed acquisition of full spectra, each SIF could be analyzed. The BZT molecule has a grouping of peaks around ~1000 cm^{-1} and another dominant peak around ~1570 cm^{-1}. The SERS spectrum shown in Figure 1c and a Raman spectrum of neat BZT liquid shown in Figure S8 show these well-defined peaks. The BZT molecule also has peaks in the ~1300 cm^{-1} range, but they are much weaker.[25] However, carbon contamination will have a strong peak around ~1300 cm^{-1}. Therefore, by examining the spectrum of each SIF event, we could exclude SIFs that had a large ~1300 cm^{-1} peak which could suggest carbon contamination due to photodecomposition. While fewer events were therefore analyzed and it is likely that events from an intact probe molecule were also rejected, this strict grouping of SIF events based on detected spectral features allows more confidence that the SIF is from a single-molecule SERS event. This type of sorting of high-speed SIF behavior is made possible by capturing the entire spectrum. While hotspot dynamics would also be relevant to fluctuations of the carbon signals from the surface, the concept of single-molecule SERS is no longer relevant.

With this spectral filtering step, Figure 5e shows a distribution of the detected SIF durations, for both the 10^4 and the 10^5 acquisition rates (spectra per second). Due to the limited number of continuous acquisitions, each rate can only detect SIF events up to a maximum duration. However, Figure 5e shows that the SIF events cover a wide range of timescales, from 10s of μs to 10s of ms. The peak widths can also be examined, as shown in Figure 5f, for all SIFs detected at the 10^4 acquisition rate. The detected peak widths are generally narrow, i.e., within the ~100 cm^{-1} resolution of the spectrometer and as indicated by the horizontal dashed line, but there is a wide range of peak widths, with some detected peaks covering an ~1000 cm^{-1} range. There is also a consistently broad peak intersecting the shoulders of the notch filter near −500 cm^{-1}. Excluding this peak from a tally reveals that 66% of all the detected SERS peaks were "narrow" and the remaining peaks were "wide" as marked and are likely the broad "flares" as shown in Figure 3 or broad increases in the background level.

Figure 5g shows a histogram of the relative change in the center of intensity, or the weighted average wavenumber, of the entire SERS spectrum for each SIF. This is done using two different laser powers of ~0.5 and ~1.0 mW at the sample. Plotting the SIF data in this way determines which portion of the spectrum during a SIF event had the largest change from the average or background SERS spectrum. Three regions can be defined in the histogram corresponding to SIF events that occurred primarily in the Stokes region, primarily in the anti-Stokes region, or in both simultaneously. These correspond to the types of SIFs shown earlier in Figure 4f,h,b, respectively. The SIF regions were defined as the change in center of intensity being greater than +100 cm^{-1} for a "Stokes" type event, less than −100 cm^{-1} for an "anti-Stokes" type event, and between −100 cm^{-1} and +100 cm^{-1} for a "Both" type event. These percentages correspond roughly to the shoulders or one standard deviation from the mean of the histograms and provide a simple metric as to where the SIF occurred spectrally. Interestingly, since the histogram is nearly symmetric, it shows that neither the Stokes nor the anti-Stokes side of the spectrum was favored to fluctuate as a SIF. Of all the SIFs recorded at the 10^4 acquisition rate with the lower laser power, 83% of the SIFs were simultaneous Stokes and anti-Stokes events, 6% of the SIFs were Stokes only events, and 11% of the SIFs were anti-Stokes only events. This is similar to the higher laser power. Indeed, there does not appear to be a large laser power dependence on the overall spectral locations of the SIF events, except that larger powers can lead to detecting SIFs that occur further from the laser line, i.e., a slightly broader distribution, perhaps due to increased signal intensity overall. These data suggest that, rather than heavily favoring one side of the spectrum over the other, the spectral location of the SIF events are much more uniformly distributed. The results in Figure 5 imply that the generation of dynamic hotspots during SERS will support resonances over a very wide range, on both sides of the laser line. While the overall intensity of the Stokes region is generally quite a bit higher than the anti-Stokes region, the probability that either region will fluctuate to generate a SIF is more symmetrical.

Figure 5h shows a histogram of the average anti-Stokes to Stokes ratio $\frac{\overline{I_{aS}}}{\overline{I_S}}$ for each SIF, where $\overline{I_{aS}}$ and $\overline{I_S}$ are the average intensities of the anti-Stokes and the Stokes regions, respectively, over the ~300 to ~2200 cm^{-1} range. Two histograms are plotted with two different laser powers. On average, the higher laser power produced SIFs with a larger anti-Stokes/Stokes ratio, represented by the positive shift of the distribution. However, the distributions are very broad, and both laser powers had a significant probability of generating a SIF with $\frac{\overline{I_{aS}}}{\overline{I_S}}$ on the order of 1/10 or more. Considering the height of a single Raman peak, a simple thermodynamic equilibrium model would associate the ratio of the anti-Stokes peak intensity I_{aS} to the Stokes peak intensity I_S to the temperature[44] of the molecule using the following:

$$\frac{I_{aS}}{I_S} = \frac{(\nu_L + \nu_R)^3}{(\nu_L - \nu_R)^3} \exp[-h\nu_R/k_B T]$$

where ν_R is the Raman shift frequency of the Stokes and anti-Stokes resonances, ν_L is the frequency of the illumination laser, h is Planck's constant, k_B is Boltzmann's constant, and T is the absolute temperature. For an ~1000 cm^{-1} peak excited at room temperature, this ratio is expected to be on the order of 1/100. For the ±1570 cm^{-1} peaks, this would be more like 1/1200. Averaging over the ~300 to ~2200 cm^{-1} range, as done with the data above, would produce a ratio $\frac{\overline{I_{aS}}}{\overline{I_S}}$ of roughly 0.031. Figure S8 shows a Raman spectrum of neat BZT liquid with the expected thermal equilibrium anti-Stokes/Stokes ratio. In this case, the ratio of the average intensities of the anti-Stokes to the Stokes regions $\frac{\overline{I_{aS}}}{\overline{I_S}}$ is measured to be 0.027, close to the expected thermal equilibrium value. This is shown as the vertical dashed line in Figure 5h. However, in our SERS experiments, the majority of SIFs have an average anti-Stokes/Stokes ratio much larger than this value, closer to ~0.1 and sometimes even greater than one. For SIF events captured at lower laser power, 0.5% had an anti-Stokes/Stokes ratio greater than 1.0. This was 0.9% at the higher laser power. While there is heating of the molecule due to laser illumination as discussed above and the increase in the anti-Stokes to Stokes ratio shows this effect, the simple model of a single molecule entering a single hotspot does not fully explain these relative intensities of the anti-Stokes and the Stokes regions. Indeed, a ratio of ~1 for the ±1570 cm^{-1} peaks, as shown in Figure 5b, would predict an unrealistically high temperature of ~4000 K. The temperature associated with the broad anti-Stokes SIF of Figure 4h would also be unrealistically high. Since there is a wide distribution of ratios for all the SIF events, with many having an anomalously large value, there must

https://doi.org/10.1021/acsnano.2c12457
ACS Nano 2023, 17, 6675−6686

therefore be a spectral component to the efficiency of the SERS hotspot that could preferentially enhance various portions of the spectrum.[35,36,45] Experiments done with a scanning tip have also demonstrated a similar effect.[46] Since Figure 5g showed that rapid SIF events are equally probable on both sides of the laser line and can enhance a single portion of the SERS spectrum or the full spectrum, all on μs to ms timescales, experiments done at slower speeds may not fully capture important information regarding the nature of single-molecule SERS.

CONCLUSION

We developed an experimental system for recording SERS spectra at speeds of up to 100,000 spectra per second. Spectral fluctuations and high-speed dynamics were seen in the single-molecule SERS signals. Examining both the Stokes and the anti-Stokes regions of the spectra at high speeds demonstrated a few results. First, there did not appear to be a significant preference as to whether the Stokes region or the anti-Stokes region would fluctuate at high speeds. The submillisecond high-speed hotspot dynamics are equally likely to appear anywhere in the spectrum. This indicates the production of SERS hotspots over a wide spectral range with varying spectral widths. Second, by examining the distribution of peak widths, approximately two-thirds of the detected peaks during all SIF events were narrow SERS lines, while the remaining one-third were broad peaks. This suggests that high-speed SERS activity and high-speed "flare" or "luminescence" activity of the silver, at least under the experimental conditions examined here, occur with probabilities of the same order of magnitude. Lastly, while the Stokes region of the spectrum is almost always greater in intensity than the anti-Stokes region, SIF events in the anti-Stokes region can create large amplifications of the anti-Stokes side for brief periods. These events were rare, and capturing a SIF with an average anti-Stokes to Stokes ratio greater than 1.0 happened in less than 1% of the detected SIF events. These results show the utility of high-speed spectral characterization to provide further insights in the SERS effect and its potential applications.

METHODS

To fabricate the SERS samples, silica nanospheres (Bang's Laboratories) were drop coated onto a glass coverslip in a 1000:1 H_2O:NS solution. The samples were allowed to evaporate for self-assembly of a hexagonal packed surface and then covered with a 300 nm thick film of silver (99.99%, R. D. Mathis) in a thermal deposition chamber (Oxford Vacuum Science, VaporStation) with typical deposition rates of ~25 nm/s. The samples were then immediately incubated in a 100 nM solution of benzenethiol (BZT, Sigma-Aldrich) in ethanol for 24 h. The samples were rinsed in ethanol and dried under filtered air. While the samples were typically measured right away in an inverted microscope system (Nikon) with several laser excitation and detector options, they remained relatively stable and gave similar signals even after a few days of storage. For all SERS measurements, a 660 nm red excitation laser (Gem 660, Laser Quantum) was used. Our microscope used a Chroma notched beam splitter (ZT656dcrb) with an optical density (OD) of ~1.7 centered at 656 nm in the blocking region and transmission of ~95% in the unblocked region. The width of the blocking region was 30 nm. We also used a Thorlabs notch filter (NF658-26) centered at 658 nm with an OD of ~6.0 to collect the full SERS spectrum. The width of the blocking region was ~26 nm, and transmission in the unblocked region was >95%. All spectra were recorded on an electron-multiplied (EM) CCD camera (iXon 888, Andor) attached to a compact imaging spectrometer (MicroHR, Horiba) with a 100 line/mm blazed diffraction grating. The EMCCD camera was deep-cooled to −70 °C and has an adjustable gain to enable operation in a single-photon counting mode with very low noise. Custom LabVIEW software was created to operate the camera in the high-speed mode as described in the text. Specifically, the Software Development Kit (SDK) from Andor with included LabVIEW drivers was used to communicate with the Andor iXon 888 EMCCD camera and configure the camera into its "Fast Kinetics" readout mode. This enabled the high-speed, row-by-row pixel shifting. It was critical that light only fell on the 8-by-1024 strip of pixels as discussed in the text, since the rest of the CCD array was used for temporary storage before the entire 1024-by-1024 image was read out at normal video rates. Our software was built on this "Fast Kinetics" feature of the camera hardware and provided a user interface for the capture of the sequence of images, file saving and numbering, and other features such as a live focusing mode for running the experiments. Laser powers at the sample varied from ~0.1 to ~1.0 mW as described in the main text. SERS analysis and SIF event detection consisted of using an "anomaly detection" algorithm written in MATLAB and as described by us elsewhere.[19] The extracted SIF data was processed further in MATLAB for plotting. Near-field scanning optical microscope (NSOM) images were created with a Nanonics MultiView 4000 with a 638 nm fiber-coupled laser (Thorlabs). The NSOM probes were fiber-coupled with a 200 nm aperture to collect the SERS signals with a photon counting module (Excelitas) after passing through a steep long-pass filter (Thorlabs).

ASSOCIATED CONTENT

Supporting Information

The Supporting Information is available free of charge at https://pubs.acs.org/doi/10.1021/acsnano.2c12457.

Additional data and descriptions of the samples, Raman spectra, laser power effects, and the peak-finding algorithm (PDF)

AUTHOR INFORMATION

Corresponding Authors

Alexandre G. Brolo − *Department of Chemistry, University of Victoria, Victoria, British Columbia V8P 5C2, Canada;* orcid.org/0000-0002-3162-0881; Email: agbrolo@uvic.ca

Nathan C. Lindquist − *Department of Physics and Engineering, Bethel University, St. Paul, Minnesota 55112, United States;* orcid.org/0000-0002-1226-5212; Email: n-lindquist@bethel.edu

Authors

Makayla M. Schmidt − *Department of Physics and Engineering, Bethel University, St. Paul, Minnesota 55112, United States*

Emily A. Farley − *Department of Physics and Engineering, Bethel University, St. Paul, Minnesota 55112, United States*

Marit A. Engevik − *Department of Physics and Engineering, Bethel University, St. Paul, Minnesota 55112, United States*

Trey N. Adelsman − *Department of Physics and Engineering, Bethel University, St. Paul, Minnesota 55112, United States*

Ariadne Tuckmantel Bido − *Department of Chemistry, University of Victoria, Victoria, British Columbia V8P 5C2, Canada*

Nathan D. Lemke − *Department of Physics and Engineering, Bethel University, St. Paul, Minnesota 55112, United States;* orcid.org/0000-0003-4165-0715

Complete contact information is available at: https://pubs.acs.org/10.1021/acsnano.2c12457

Author Contributions

$^{\nabla}$M.M.S., E.A.F., and M.A.E. contributed equally.

https://doi.org/10.1021/acsnano.2c12457
ACS Nano 2023, 17, 6675−6686

Notes

The authors declare no competing financial interest.

ACKNOWLEDGMENTS

N.C.L. and N.D.L. acknowledge support from the National Science Foundation (NSF) award #2003750. A.G.B. acknowledges operational grant support from the Natural Sciences and Engineering Research Council of Canada (NSERC) and instrument grant support from the Canada Foundation for Innovation (CFI), the British Columbia Knowledge Development Fund (BCKDF), and the University of Victoria.

REFERENCES

(1) Maccaferri, N.; Barbillon, G.; Koya, A. N.; Lu, G.; Acuna, G. P.; Garoli, D. Recent Advances in Plasmonic Nanocavities for Single-Molecule Spectroscopy. *Nanoscale Adv.* **2021**, *3*, 633−642.

(2) Brolo, A. G. Plasmonics for Future Biosensors. *Nat. Photonics* **2012**, *6*, 709−713.

(3) Baffou, G.; Quidant, R. Nanoplasmonics for Chemistry. *Chem. Soc. Rev.* **2014**, *43*, 3898−3907.

(4) Dong, B.; Ma, Y.; Ren, Z.; Lee, C. Recent Progress in Nanoplasmonics-Based Integrated Optical Micro/Nano-Systems. *J. Phys. D: Appl. Phys.* **2020**, *53*, 213001.

(5) Sundararaman, R.; Christensen, T.; Ping, Y.; Rivera, N.; Joannopoulos, J. D.; Soljacić, M.; Narang, P. Plasmonics in Argentene. *Phys. Rev. Mater.* **2020**, *4*, 074011.

(6) Langer, J.; Jimenez de Aberasturi, D.; Aizpurua, J.; Alvarez-Puebla, R. A.; Auguié, B.; Baumberg, J. J.; Bazan, G. C.; Bell, S. E.; Boisen, A.; Brolo, A. G.; Choo, J.; Cialla-May, D.; Deckert, V.; Fabris, L.; Faulds, K.; García de Abajo, F. J.; Goodacre, R.; Graham, D.; Haes, A. J.; Haynes, C. L.; et al. Present and Future of Surface-Enhanced Raman Scattering. *ACS Nano* **2020**, *14*, 28−117.

(7) Fan, M.; Andrade, G. F.; Brolo, A. G. A Review on Recent Advances in The Applications of Surface-Enhanced Raman Scattering in Analytical Chemistry. *Anal. Chim. Acta* **2020**, *1097*, 1−29.

(8) Pérez-Jiménez, A. I.; Lyu, D.; Lu, Z.; Liu, G.; Ren, B. Surface-Enhanced Raman Spectroscopy: Benefits, Trade-Offs and Future Developments. *Chem. Sci.* **2020**, *11*, 4563−4577.

(9) Nie, S.; Emory, S. R. Probing Single Molecules and Single Nanoparticles By Surface-Enhanced Raman Scattering. *Science* **1997**, *275*, 1102−1106.

(10) Chikkaraddy, R.; De Nijs, B.; Benz, F.; Barrow, S. J.; Scherman, O. A.; Rosta, E.; Demetriadou, A.; Fox, P.; Hess, O.; Baumberg, J. J. Single-Molecule Strong Coupling at Room Temperature in Plasmonic Nanocavities. *Nature* **2016**, *535*, 127−130.

(11) Ding, S.-Y.; You, E.-M.; Tian, Z.-Q.; Moskovits, M. Electromagnetic Theories of Surface-Enhanced Raman Spectroscopy. *Chem. Soc. Rev.* **2017**, *46*, 4042−4076.

(12) Shin, H.-H.; Yeon, G. J.; Choi, H.-K.; Park, S.-M.; Lee, K. S.; Kim, Z. H. Frequency-Domain Proof of the Existence of Atomic-Scale SERS Hot-Spots. *Nano Lett.* **2018**, *18*, 262−271.

(13) Benz, F.; Schmidt, M. K.; Dreismann, A.; Chikkaraddy, R.; Zhang, Y.; Demetriadou, A.; Carnegie, C.; Ohadi, H.; De Nijs, B.; Esteban, R.; Aizpurua, J.; Baumberg, J. J. Single-Molecule Optomechanics in "Picocavities. *Science* **2016**, *354*, 726−729.

(14) Fan, M.; Andrade, G. F.; Brolo, A. G. A Review on The Fabrication Of Substrates for Surface Enhanced Raman Spectroscopy and Their Applications in Analytical Chemistry. *Anal. Chim. Acta* **2011**, *693*, 7−25.

(15) Santinom, A.; da Silva, M. A.; Villa, J. E.; Poppi, R. J.; Mazali, I. O.; dos Santos, D. P. Surface-Enhanced Raman Scattering (SERS) as Probe of Plasmonic Near-field Resonances. *Vib. Spectrosc.* **2018**, *99*, 34−43.

(16) Bantz, K. C.; Meyer, A. F.; Wittenberg, N. J.; Im, H.; Kurtulus, Ö.; Lee, S. H.; Lindquist, N. C.; Oh, S. H.; Haynes, C. L. Recent Progress in SERS Biosensing. *Phys. Chem. Chem. Phys.* **2011**, *13*, 11551−11567.

(17) Yamamoto, Y. S.; Ishikawa, M.; Ozaki, Y.; Itoh, T. Fundamental Studies on Enhancement and Blinking Mechanism of Surface-Enhanced Raman Scattering (SERS) and Basic Applications of SERS Biological Sensing. *Frontiers of Physics* **2014**, *9*, 31−46.

(18) Margueritat, J.; Bouhelier, A.; Markey, L.; Colas des Francs, G.; Dereux, A.; Lau-Truong, S.; Grand, J.; Lévi, G.; Félidj, N.; Aubard, J.; Finot, E. Discerning the Origins of the Amplitude Fluctuations in Dynamic Raman Nanospectroscopy. *J. Phys. Chem. C* **2012**, *116*, 26919−26923.

(19) Lindquist, N. C.; de Albuquerque, C. D. L.; Sobral-Filho, R. G.; Paci, I.; Brolo, A. G. High-Speed Imaging of Surface-Enhanced Raman Scattering Fluctuations from Individual Nanoparticles. *Nat. Nanotechnol.* **2019**, *14*, 981−987.

(20) de Albuquerque, C. D. L.; Hokanson, K. M.; Thorud, S. R.; Sobral-Filho, R. G.; Lindquist, N. C.; Brolo, A. G. Dynamic Imaging of Multiple SERS Hotspots on Single Nanoparticles. *ACS Photonics* **2020**, *7*, 434−443.

(21) Bido, A. T.; Nordberg, B. G.; Engevik, M. A.; Lindquist, N. C.; Brolo, A. G. High-Speed Fluctuations in Surface-Enhanced Raman Scattering Intensities from Various Nanostructures. *Appl. Spectrosc.* **2020**, *74*, 1398−1406.

(22) Lindquist, N. C.; Bido, A. T.; Brolo, A. G. Single-Molecule SERS Hotspot Dynamics in Both Dry and Aqueous Environments. *J. Phys. Chem. C* **2022**, *126*, 7117−7126.

(23) Lombardi, J. R.; Birke, R. L.; Haran, G. Single Molecule SERS Spectral Blinking and Vibronic Coupling. *J. Phys. Chem. C* **2011**, *115*, 4540−4545.

(24) Lindquist, N. C.; Brolo, A. G. Ultra-High-Speed Dynamics in Surface-Enhanced Raman Scattering. *J. Phys. Chem. C* **2021**, *125*, 7523−7532.

(25) Madzharova, F.; Heiner, Z.; Kneipp, J. Surface-Enhanced Hyper Raman Spectra of Aromatic Thiols on Gold and Silver Nanoparticles. *J. Phys. Chem. C* **2020**, *124*, 6233−6241.

(26) Wang, K.; Schonbrun, E.; Steinvurzel, P.; Crozier, K. B. Trapping and Rotating Nanoparticles Using a Plasmonic Nano-Tweezer with an Integrated Heat Sink. *Nat. Commun.* **2011**, *2*, 469−474.

(27) Carnegie, C.; Urbieta, M.; Chikkaraddy, R.; de Nijs, B.; Griffiths, J.; Deacon, W. M.; Kamp, M.; Zabala, N.; Aizpurua, J.; Baumberg, J. J. Flickering Nanometre-Scale Disorder in a Crystal Lattice Tracked by Plasmonic Flare Light Emission. *Nat. Commun.* **2020**, *11*, 1−9.

(28) Hu, H.; Duan, H.; Yang, J. K.; Shen, Z. X. Plasmon-Modulated Photoluminescence of Individual Gold Nanostructures. *ACS Nano* **2012**, *6*, 10147−10155.

(29) Lin, K.-Q.; Yi, J.; Hu, S.; Sun, J.-J.; Zheng, J.-T.; Wang, X.; Ren, B. Intraband Hot-Electron Photoluminescence from Single Silver Nanorods. *ACS Photonics* **2016**, *3*, 1248−1255.

(30) Hugall, J. T.; Baumberg, J. J. Demonstrating Photoluminescence from Au Is Electronic Inelastic Light Scattering of a Plasmonic Metal: The Origin of SERS Backgrounds. *Nano Lett.* **2015**, *15*, 2600−2604.

(31) Mertens, J.; Kleemann, M.-E.; Chikkaraddy, R.; Narang, P.; Baumberg, J. J. How Light Is Emitted by Plasmonic Metals. *Nano Lett.* **2017**, *17*, 2568−2574.

(32) Weber, M. L.; Litz, J. P.; Masiello, D. J.; Willets, K. A. Super-Resolution Imaging Reveals a Difference Between SERS and Luminescence Centroids. *ACS Nano* **2012**, *6*, 1839−1848.

(33) Lin, K.-Q.; Yi, J.; Zhong, J.-H.; Hu, S.; Liu, B.-J.; Liu, J.-Y.; Zong, C.; Lei, Z.-C.; Wang, X.; Aizpurua, J.; Esteban, R.; Ren, B. Plasmonic Photoluminescence for Recovering Native Chemical Information from Surface-Enhanced Raman Scattering. *Nat. Commun.* **2017**, *8*, 14891.

(34) Chen, W.; Roelli, P.; Ahmed, A.; Verlekar, S.; Hu, H.; Banjac, K.; Lingenfelder, M.; Kippenberg, T. J.; Tagliabue, G.; Galland, C. Intrinsic Luminescence Blinking from Plasmonic Nanojunctions. *Nat. Commun.* **2021**, *12*, 1−9.

(35) Dos Santos, D. P.; Temperini, M. L.; Brolo, A. G. Mapping the Energy Distribution of SERRS Hot Spots From Anti-Stokes To Stokes Intensity Ratios. *J. Am. Chem. Soc.* **2012**, *134*, 13492−13500.

(36) Brolo, A.; Sanderson, A.; Smith, A. Ratio of The Surface-Enhanced Anti-Stokes Scattering to the Surface-Enhanced Stokes-Raman Scattering for Molecules Adsorbed On a Silver Electrode. *Phys. Rev. B* **2004**, *69*, 045424.

https://doi.org/10.1021/acsnano.2c12457
ACS Nano 2023, 17, 6675−6686

(37) Lee, J.; Crampton, K. T.; Tallarida, N.; Apkarian, V. A. Visualizing Vibrational Normal Modes of A Single Molecule with Atomically Confined Light. *Nature* **2019**, *568*, 78.
(38) Pozzi, E. A.; Zrimsek, A. B.; Lethiec, C. M.; Schatz, G. C.; Hersam, M. C.; Van Duyne, R. P. Evaluating Single-Molecule Stokes and Anti-Stokes SERS For Nanoscale Thermometry. *J. Phys. Chem. C* **2015**, *119*, 21116−21124.
(39) Haslett, T.; Tay, L.; Moskovits, M. Can Surface-Enhanced Raman Scattering Serve as a Channel for Strong Optical Pumping? *J. Chem. Phys.* **2000**, *113*, 1641−1646.
(40) Kneipp, K.; Wang, Y.; Kneipp, H.; Itzkan, I.; Dasari, R. R.; Feld, M. S. Population Pumping of Excited Vibrational States by Spontaneous Surface-Enhanced Raman Scattering. *Phys. Rev. Lett.* **1996**, *76*, 2444.
(41) Maher, R.; Cohen, L.; Gallop, J.; Le Ru, E.; Etchegoin, P. Temperature-Dependent Anti-Stokes/Stokes Ratios Under Surface-Enhanced Raman Scattering Conditions. *J. Phys. Chem. B* **2006**, *110*, 6797−6803.
(42) Kudelski, A.; Pettinger, B. SERS On Carbon Chain Segments: Monitoring Locally Surface Chemistry. *Chem. Phys. Lett.* **2000**, *321*, 356−362.
(43) Domke, K. F.; Zhang, D.; Pettinger, B. Enhanced Raman Spectroscopy: Single Molecules or Carbon? *J. Phys. Chem. C* **2007**, *111*, 8611−8616.
(44) Kip, B. J.; Meier, R. J. Determination of The Local Temperature at a Sample During Raman Experiments Using Stokes and Anti-Stokes Raman Bands. *Appl. Spectrosc.* **1990**, *44*, 707−711.
(45) Dos Santos, D. P.; Temperini, M. L.; Brolo, A. G. Single-Molecule Surface-Enhanced (Resonance) Raman Scattering (SE (R) RS) as a Probe for Metal Colloid Aggregation State. *J. Phys. Chem. C* **2016**, *120*, 20877−20885.
(46) Richard-Lacroix, M.; Deckert, V. Direct Molecular-Level Near-Field Plasmon and Temperature Assessment in a Single Plasmonic Hotspot. *Light: Sci. Appl.* **2020**, *9*, 1−13.

https://doi.org/10.1021/acsnano.2c12457
ACS Nano 2023, 17, 6675−6686